Dual-polarized Fixed-frequency Beam Scanning Leaky-wave Antenna for 5G Communication

Hao Xiang Li [1] and Yong Jin Zhou [1,2,*]

[1] Key Laboratory of Specialty Fiber Optics and Optical Access Networks
Shanghai University, Shanghai 200444, China

[2] State Key Laboratory of Millimeter Waves, Southeast University, Nanjing 210096, China
*yjzhou@shu.edu.cn

Abstract ─ A low profile and dual-polarized fixed-frequency beam scanning leaky wave antenna for 5G communication is presented, which is based on a corrugated microstrip line (CML) called spoof surface plasmons transmission line. The antenna radiates horizontally polarized electromagnetic wave and vertically polarized electromagnetic wave using two different periodic antennas elements. The fabricated antenna is measured and the results show that the operating frequency of the antenna is 3.4-3.7 GHz. The measured main beam angle scans from -9° to -30°. The measured gain is from 8.3 dB to 9.7 dB over the working band.

Index Terms ─Spoof surface plasmons, 5G, dual-polarized, fixed-frequency

I. INTRODUCTION

The commercialization of the fifth generation mobile communication system (5G) puts forward many high performance requirements for the communication system [1]. As a crucial part of the communication system, the breakthrough of the antenna will obviously improve the performance of the whole communication system. The traditional beam scanning antenna usually uses frequency scanning mechanism or phase shifter to realize beam scanning, which will inevitably bring the problem of occupying wide-band spectral resources and complex feeding network structure, thus increasing the volume and cost of the whole system [2].

Leaky wave antennas (LWA) have advantages of high gain, frequency scanning features, and a simple feeding structure. The combination of metamaterials and traditional leaky wave antennas results in low profile, high gain, low cost leaky wave antennas, which emerged as potential candidates in modern wireless communication system [3,4]. The metamaterial leaky wave antennas can be divided into two kinds. One kind is based on the composite right-/left-handed (CRLH) transmission line and the other is based on the spoof surface plasmons (SPs) [5,6]. By constructing CRLH transmission line design in the balance, researchers concluded that CRLH leaky wave antennas can overcome the open-stopband effects [7,8]. Different devices based on spoof SPs at millimeter wave and terahertz frequencies have been demonstrated [9-12]. The spoof SPs LWA can radiate spatial harmonics by introducing periodic modulations [13-17]. However, previous metamaterial leaky wave antennas occupy wide-band frequency resources in the frequency scanning process, hence most of the above metamaterial leaky wave antennas are generally designed for satellite communication (working at high frequency band) or radar detection to carry out large-angle scanning, which are not suitable for 5G communication system with relatively narrow operating bands [18,19]. Therefore, how to complete beam scanning metamaterial LWA at fixed-frequency is an important research area.

In recent years, researchers have achieved beam scanning metamaterial leaky-wave antennas at fixed frequencies by loading PIN-diodes or varactor diodes [20-24]. For example, single-polarized fixed-frequency beam scanning antennas based on spoof SPs have been proposed [20-21], respectively. However, these beam scanning antennas still are single-polarized, which does not meet the requirements of 5G communication system, since dual-polarized antenna in the communication system is necessary. Especially in 5G communication systems, large-scale antenna arrays are generally adopted, which requires the polarization diversity. Therefore, the study of dual-polarized fixed-frequency beam scanning antenna is important [25-26].

In this work, we propose a dual-polarized beam scanning antenna as shown in Fig. 1. The dispersion curve of the antenna unit is adjusted by loading a varactor diode to complete the beam scanning at a fixed-frequency. The working frequency band is located in 3.4-3.7 GHz for 5G communication. The maximum gain can reach 10 dB in the working frequency band, and the rotation angle at the 3.5 GHz is about 21°.

Submitted On: February 7, 2021
Accepted On: July 6, 2021

https://doi.org/10.47037/2021.ACES.J.360706

Compared with previous leaky wave antennas, the proposed antenna has the advantages of dual polarization, low profile and beam scanning at a fixed frequency.

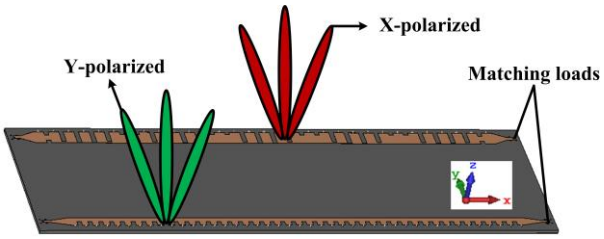

Fig. 1. A dual-polarized beam scanning LWA.

II. ANTENNA DESIGN

A. The design of X-polarized antenna

The X-polarized antenna structure with five modulation periods is shown in Fig. 2. The dimensions shown in Fig. 2 (a) are od = 13 mm, op = 6od = 78 mm, w_1 = 0.6 mm, w_2 = 2.1 mm, h_4 = 15 mm, tl_1 = 0.7od, and tl_2 = 0.3od. The groove depths are h_1 = 3.137 mm, h_2 = 13.164 mm, h_3 = 14.51 mm, respectively. The schematic of the LWA with sinusoidally modulated surface impedance is shown in Fig. 2 (b), which is composed of a corrugated metallic strip line, dielectric substrate and metallic ground, where the dielectric substrate is F4B with relative permittivity 3.5 and loss tangent 0.001. The thicknesses of dielectric substrate and the metal are 3 mm and 0.018 mm, respectively. The total length of the LWA is 440 mm.

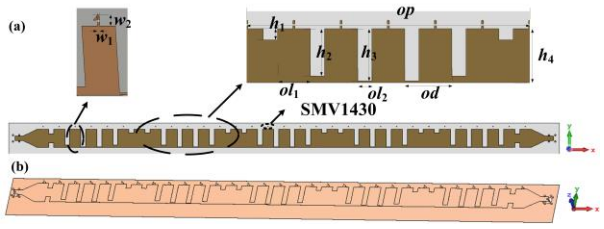

Fig. 2. (a) The details of X-polarized antenna, and (b) the perspective of X-polarized antenna (the dielectric substrate is transparent).

The radiation principle of X-polarized antenna with different grooves is that the surface impedance changes result in the formation of space radiation. The radiated electric field is always perpendicular to the groove [20]. Hence, the direction of its polarization is along the X-axis (X-polarized antenna).

According to the leaky-wave antenna theory, the surface impedance of the antenna is modulated periodically according to the sine function, as shown in Equation (1),

$$Z_s(x) = jX_s[1 + M\cos(\frac{2\pi x}{p})], \tag{1}$$

where X_s, M, and p are the average surface reactance, modulation factor, and the modulation period, respectively.

From the Floquet theorem, the surface wave propagating on the impedance will excite infinite high-order spatial harmonics, as shown in Equation (2):

$$\beta_N p = \beta_0 + 2\pi n, \tag{2}$$

where β_0 is the phase constant of the fundamental space harmonic with N = 0 and β_N is the phase constant of N-order.

These higher spatial harmonics can be surface waves propagating along the surface or leakage waves radiating into free space. The mode of these high-order spatial harmonics mainly depends on the modulation period. The first negative harmonic mode is usually designed to generate the leaky-wave radiation, whose radiation angle can be calculated by Equation (3),

$$\theta \approx \sin^{-1}(\sqrt{1 + X'^2} - \frac{2\pi}{k_0 p}), \tag{3}$$

where X' = X_s/η_0 is the normalized average surface reactance and k_0 is the propagation constant of free space.

The simulated S-parameters and gain are obtained by using CST. The simulated dispersion curves of the antenna elements with different groove depths are shown in Fig. 3. From the dispersion curve, it can be seen when h = 0 mm (unmodulated spoof SPs transmission line), the slope of the dispersion curve is the speed of light and the greater the depth of the groove is, the lower the cut-off frequency is.

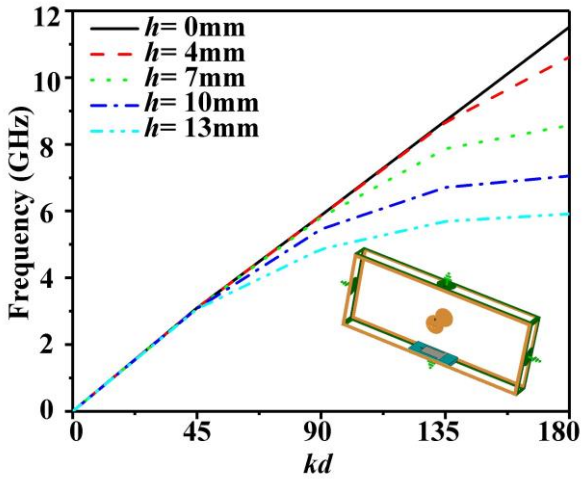

Fig. 3. The dispersion curves of the antenna elements with different groove depths.

The simulated S-parameters of the X-polarized antenna are shown in Fig. 4. It can be seen that the S_{11} is below -13 dB at 3.4-3.7 GHz, and the S_{21} is about -3 dB, which indicates that the antenna can work at 3.4-3.7 GHz.

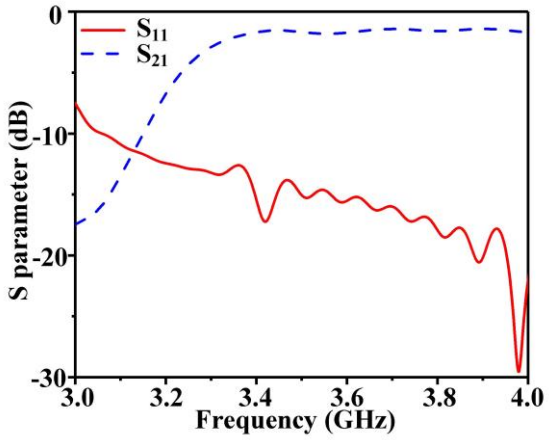

Fig. 4. The simulated S-parameters of X-polarized antenna with loaded capacitance of 0.88 pF.

The electric field of the X-polarized antenna is perpendicular to the groove. Hence, the direction of the polarization is along the X-axis [20]. The simulated far-field radiation pattern of the LWA is plotted in Fig. 5, which shows a narrow beam in E-plane (*xoz* plane) plane with low back lobes. The level of the cross polarization (Y polarization) is also low. By loading the SMV1430-040LF varactor diode, the X-polarized antenna can complete beam scanning at a fixed frequency.

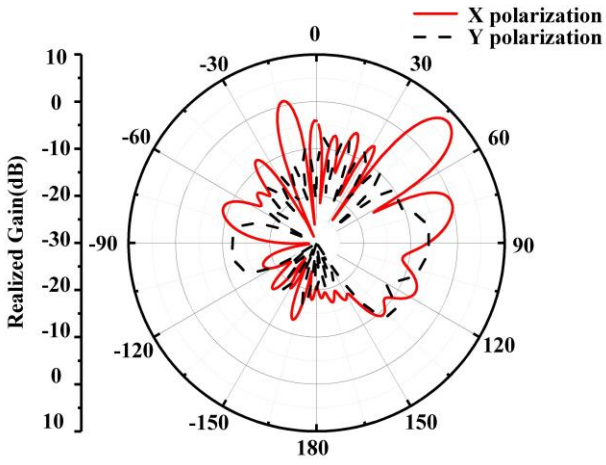

Fig. 5. Simulated far-field radiation pattern of the X-polarized antenna at 3.7 GHz with loaded capacitance of 0.88 pF.

B. The design of Y-polarized antenna

The radiation principle of the Y-polarized antenna is different from that of X-polarized antenna. By loading different capacitors periodically, the Y-polarized antenna radiates electromagnetic waves into space. The radiation principle of the antenna with same grooves is that the surface impedance changes due to different capacitances. So the electric field of the antenna is always along the loading capacitance [21]. It is along Y-axis direction (Y-polarized antenna). The Y-polarized antenna has seven modulation periods, as shown in Fig. 6. The geometric parameters shown in Fig. 6 (a) are td = 9.2 mm, tp = 6td = 55.2 mm, h_5 = 10 mm, tl_1 = 0.6td, and tl_2 = 0.4td.

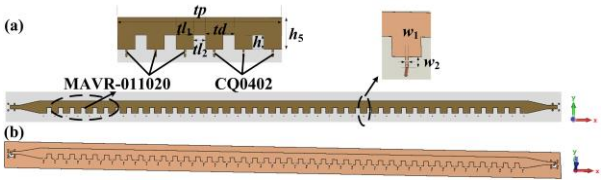

Fig. 6. (a) The details of Y-polarized antenna, and (b) the perspective view of the Y-polarized antenna.

The modulation period consists of six sub-wavelength units, and these sub-wavelength units loaded with three identical fixed capacitors and varactor diodes to periodically change the surface impedance. The surface impedance modulation principle of Y-polarized antenna can be equivalent to the triangular impedance modulation principle as shown in Equation (4):

$$Z_s(x)=\begin{cases} jX_s(1+\dfrac{2M}{p}x-\dfrac{M}{2}) & if\ 0\le x\le \dfrac{p}{2} \\ jX_s(1-\dfrac{2M}{p}x+\dfrac{3M}{2}) & if\ \dfrac{p}{2}\le x\le p \end{cases}, \quad (4)$$

where X_s, M, and p are the average surface reactance, modulation factor and the modulation period, respectively. The surface impedance of the antenna unit is changed by periodically changing the capacitance, so the direction of electric field change is always perpendicular to the groove where the capacitance is loaded.

The simulation setting of one unit cell of the Y-polarized antenna is shown in Fig. 7 (a), where periodic boundary condition (PBC) is used in x direction and perfect electric conductor condition (PEC) is used in y direction. The Eigenmode Solver of the commercial software CST Microwave Studio is adopted. However, the lumped capacitor cannot be added in the Eigenmode Solver of CST Microwave Studio. Hence, an equivalent model is used to take place of the lumped capacitor in the simulations. The equivalent model consists of two metallic slabs spaced by a dielectric block. The

permittivity of the dielectric block can be calculated by $\varepsilon_c = \varepsilon_0 \cdot b_2 \cdot C/(a_1 \cdot a_2)$, in which C is the capacitance of the lumped capacitor, and a_1, a_2, and b_2 are the dimensions illustrated in Fig. 7 (a). The simulated dispersion curves of the unit with different capacitances are shown in Fig. 7 (b). We can predict the operation band of the antenna from the dispersion curve.

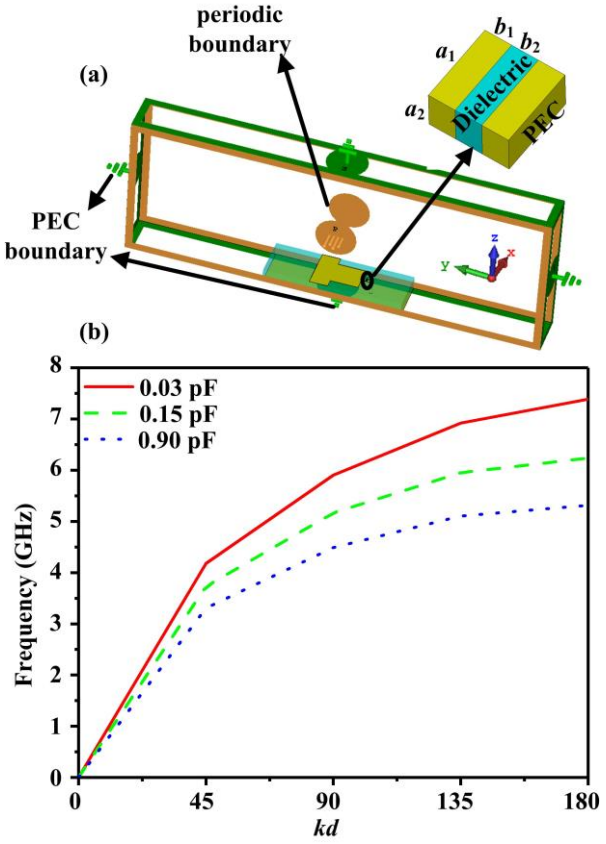

Fig. 7. (a) The details of simulation setting, and (b) the dispersion curves of the antenna elements loading different capacitors.

The simulated S-parameters of the Y-polarized antenna are shown in Fig. 8. It can be seen that the S_{11} is below -12 dB at 3.4-3.7 GHz, and the S_{21} is about -28 dB, which indicates that the antenna can effectively work at 3.4-3.7 GHz. Compared with Fig. 4, it can be seen that the S_{21} performs better in Fig. 8 for the Y-polarized antenna. That is because that the impedance changes caused by periodic loaded capacitors are more drastic than those caused by different groove depths, which leads to more leaky wave radiation energy of the Y-polarized antenna. Therefore, the S_{21} of the Y-polarized antenna performs better than that of the X-polarized antenna.

Furthermore, the simulated far-field radiation pattern of the LWA is plotted in Fig. 9, which shows a narrow beam in E-plane (xoz plane) with low back lobes. The level of the X polarization is also low. By periodically loading the varactor diodes (MAVR-011020-1411) and the fixed capacitors (CQ0402BRNPO9BN1R1), the Y-polarized antenna completes beam scanning at a fixed frequency.

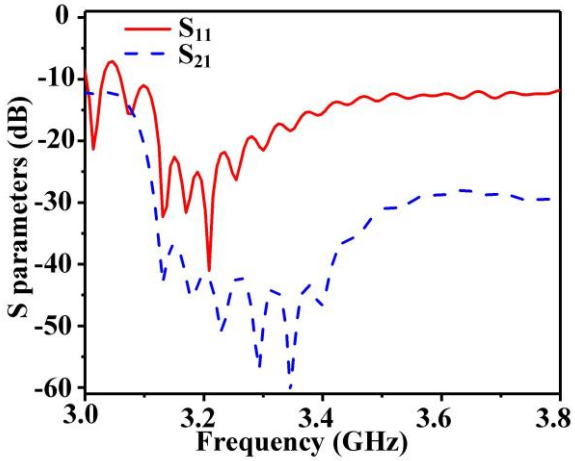

Fig. 8. The simulated S-parameters of Y-polarized antenna with loaded capacitance of 0.15 pF.

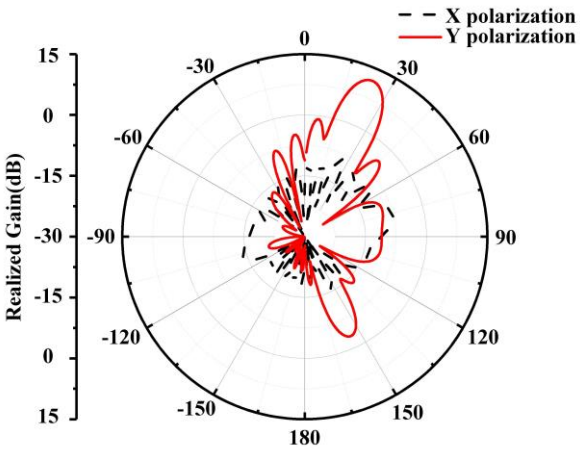

Fig. 9. The simulated far-field radiation pattern of the Y-polarized antenna at 3.7 GHz with loaded capacitance of 0.15 pF.

C. The design of dual-polarized antenna

We combine the X-polarized antenna and the Y-polarized antenna to form the dual-polarized antenna. The simulated isolation and far-field patterns of the dual-polarized antenna are shown in Fig. 10. As can be seen from Fig. 10 (a), the isolation degree of each port is less than -35 dB. From Fig. 10 (b), it can be seen that the beam scanning dual-polarized antenna has been achieved, where the X-polarized antenna and the Y-

polarized antenna are loaded with the capacitance of 0.7pF and 0.24pF, respectively.

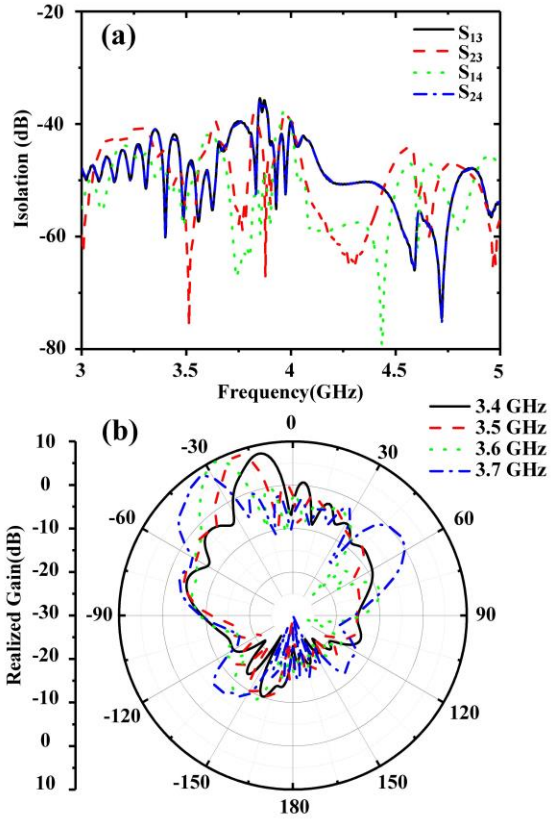

Fig. 10. (a) The isolation of the dual-polarized antenna, (b) Simulated synthesized far-field radiation pattern of the dual-polarized antenna.

III. REAULTS AND DISCUSSION

The fabricated antenna and its measurement environment are shown in Fig. 11. The dual-polarized antenna is shown in Fig. 11 (a). The final dimension of the dual-polarized antenna is 440 mm × 140 mm × 3 mm.

Fig. 11. (a) The sample of the fabricated antenna, and (b) the measurement environment.

The simulated and measured S-parameters are shown in Fig. 12. The higher the operating frequency of the active device is, the larger the influence of parasitic parameters is. The measured S_{11} and S_{21} vary drastically from their simulated results, respectively. However, the trend of simulation result agrees well to that of measurement result. Both errors are caused by the inaccurate parasitic parameters of the varactor diodes and by machining and welding.

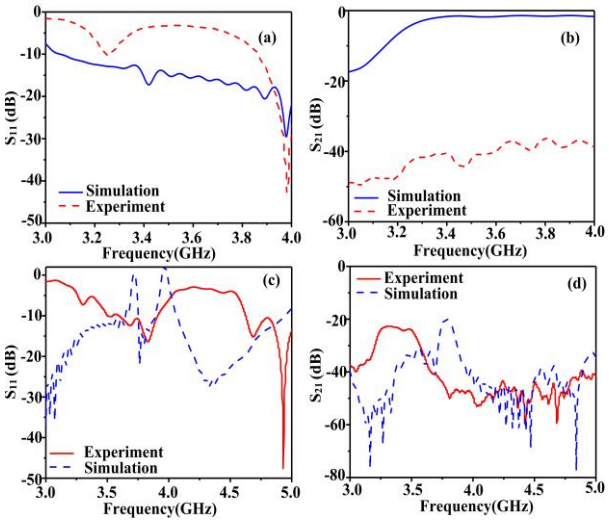

Fig. 12. The simulated and measured (a) S_{11} and (b) S_{21} of X-polarized antenna with loaded capacitance of 0.68 pF. The simulated and measured (c) S_{11} and (d) S_{21} of Y-polarized antenna with loaded capacitance of 0.15 pF.

The measured far-field radiation patterns of the dual-polarized antenna at 3.5 GHz with different voltages are shown in Fig. 13. It can be seen that when the voltage changes from 0 V to 5 V, the scanning angle is from -9° to -30° at 3.5 GHz.

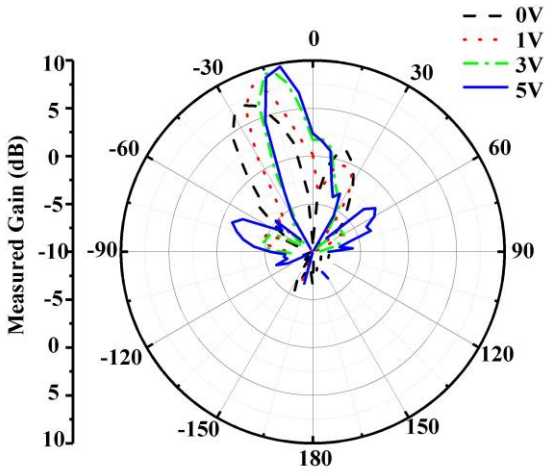

Fig. 13. The measured far-field radiation pattern of the dual-polarized antenna at 3.5 GHz with different voltages.

The simulated and measured gains of the dual-polarized antenna are shown in Fig. 14. It can be seen that the experimental results agree well with the simulation results. As the parasitic parameters of the varactor diode model are set to be typical values in simulation according to the datasheet, the actual values may be different in the lower frequency band, which results in that the actual gain at 3.3 GHz and 3.4 GHz is higher than the simulated gain.

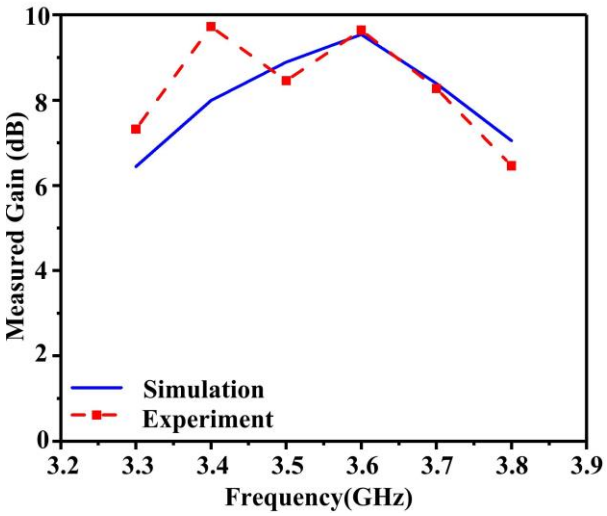

Fig. 14. The simulated and measured gain of the dual-polarized antenna.

IV. CONCLUSION

Here a dual-polarized high-gain fixed-frequency beam scanning antenna for 5G communication is proposed. By using the surface impedance modulation technology and loading the active devices, the dual-polarized antenna can achieve the fixed-frequency beam scanning at 3.4-3.7 GHz (S_{11}< -10 dB) for 5G communication systems.

ACKNOWLEDGMENT

This work was supported in part by the National Natural Science Foundation of China under Grant No. 61971469, and in part by Science and Technology Commission Shanghai Municipality (STCSM) under Grant No. 18ZR1413500, and in part by the Open Project Program of the State Key Laboratory of Millimeter Waves under Grant No. K202109.

REFERENCES

[1] K. Kaur, S. Kumar, and A. Baliyan, "5G: A new era of wireless communication," *International Journal of Information Technology*, vol. 12, pp. 619-624, June 2020.

[2] S. Rathod, K. Sreenivasulu, K. S. Beenamole, and K. P. Ray, "Evolutionary trends in transmit/receive module for active phased array radars," *Defence Science Journal*, vol. 68, pp. 553-559, 2018.

[3] A. A. Oliner, "Leakage from higher modes on microstrip line with application to antennas," *Radio Science*, vol. 22, pp. 907-912, Nov. 1987.

[4] D. R. Jackson and A. A. Oliner, "Leaky-wave antennas," in *Modern Antenna Handbook*, C. Balanis, Ed., New York, Nov. 2007.

[5] K. D. Xu, S. Lu, Y. J. Guo, and Q. Chen, "High-order mode of spoof surface plasmon polaritons and its application in bandpass filters," *IEEE Transactions on Plasma Science*, vol. 49, pp. 269-275, Mar. 2021.

[6] J. X. Li, J. W. Shi, K. D. Xu, Y. J. Guo, A. X. Zhang, and Q. Chen "Spoof surface plasmon polaritons developed from coplanar waveguides in microwave frequencies," *IEEE Photonics Technology Letters*, vol. 32, pp. 1431-1434, Oct. 2020.

[7] A. Lai, T. Itoh, and C. Caloz, "Composite right/left-handed transmission line metamaterials," *IEEE Microwave Magazine*, vol. 5, pp. 34-50, Oct. 2004.

[8] S. Rezaee and M. Memarian, "Analytical study of open-stop band suppression in leaky-wave antennas," *IEEE Antennas and Wireless Propagation Letters*, vol. 19, pp. 99, Jan. 2020.

[9] K. D. Xu, Y. J. Guo, Q. Yang, Y. L. Zhang, X. J. Deng, A. X. Zhang, and Q. Chen, "On-chip GaAs-based spoof surface plasmon polaritons at millimeter-wave regime," *IEEE Photonics Technology Letters*, vol. 33, pp. 255-258, Jan. 2021.

[10] Y. Li, J. Lin, H. Guo, W. Sun, S. Xiao, and L. Zhou, "A tunable metasurface with switchable functionalities: From perfect transparency to perfect absorption," *Advanced Optical Materials*, vol. 8, pp. 1901548, Jan. 2020.

[11] S. Xiao, F. Zhong, H. Liu, S. Zhu, and J. Li, "Flexible coherent control of plasmonic spin-Hall effect," *Nature Communications*, vol. 6, pp. 1-7, Sep. 2015.

[12] B. Yang, T. Liu, H. Guo, S. Xiao, and L. Zhou, "High-performance meta-devices based on multi-layer meta-atoms: interplay between the number of layers and phase coverage," *Science Bulletin*, vol. 64, pp. 823-835, May 2019.

[13] G. S. Kong, H. F. Ma, B. G. Cai, and T. J. Cui, "Continuous leaky-wave scanning using periodically modulated spoof plasmonic waveguide," *Scientific Reports*, vol. 6, pp. 1-9, July 2016.

[14] X. Liu, B. Chen, J. Zhang, "Frequency scanning planar antenna based on spoof surface plasmon polariton," *IEEE Antennas and Wireless Propagation Letters*, vol. 16, pp. 165-168, May 2016.

[15] H. Chen, H. Ma, Y. Li, J. Wang, Y. Han, and M. Yan, "Wideband frequency scanning SSPP planar antenna based on transmissive phase gradient

metasurface," *IEEE Antennas and Wireless Propagation Letters*, vol. 17, pp. 463-467, Jan. 2018.
[16] J. Y. Yin, J. Ren, and Q. Zhang, "Frequency-controlled broad-angle beam scanning of patch array fed by spoof surface plasmon polaritons," *IEEE Transactions on Antennas and Propagation*, vol. 64, pp. 5181-5189, Nov. 2016.
[17] D. F. Guan, P. You, and Q. Zhang, "A wide angle and circularly polarized beam scanning antenna based on microstrip spoof surface plasmon polariton transmission line," *IEEE Antennas and Wireless Propagation Letters*, vol. 16, pp. 2538-2541, July 2017.
[18] M. Ettorre, R. Sauleau, L. Le Coq, and F. Bodereau, "Single-folded leaky-wave antennas for automotive radars at 77 GHz," *IEEE Antennas and Wireless Propagation Letters*, vol. 9, pp. 859-862, Sep. 2010.
[19] F. Kozak, V. Jenik, J. Machac, and P. Hudec, "Microwave radar sensor based on CRLH siw leaky-wave antennas," *European Radar Conference*, pp. 53-56, Dec. 2014.
[20] M. Wang, H. F. Ma, H. C. Zhang, W. X. Tang, X. R. Zhang, and T. J. Cui, "Frequency-fixed beam-scanning leaky-wave antenna using electronically controllable corrugated microstrip line," *IEEE Transactions on Antennas and Propagation*, vol. 66, pp. 4449-4457, June 2018.
[21] M. Wang, H. F. Ma, W. X. Tang, H. C. Zhang, W. X. Jiang, and T. J. Cui, "A dual-band electronic-scanning leaky-wave antenna based on a corrugated microstrip line," *IEEE Transactions on Antennas and Propagation*, vol. 67, pp. 3433-3438, Mar. 2019.
[22] S. Chen, D. K. Karmokar, Z. Li, P. Qin, R. W. Ziolkowski, and Y. J. Guo, "Continuous beam scanning at a fixed frequency with a composite right-/left-handed leaky-wave antenna operating over a wide frequency band," *IEEE Transactions on Antennas and Propagation*, vol. 67, pp. 7272-7284, Aug. 2019.
[23] R. Shaw and M. K. Mandal, "Broadside scanning fixed frequency LWA with simultaneous electronic control of beam angle and beamwidth," *IEEE Transactions on Antennas and Propagation*, vol. 68, pp. 3504-3514, Feb. 2020.
[24] I. Serhsouh, M. Himdi, H. Lebbar, and H. Vettikalladi, "Reconfigurable SIW antenna for fixed frequency beam scanning and 5G applications," *IEEE Access*, vol. 8, pp. 60084-60089, Mar. 2020.
[25] H. Wang, "Capacity improvement through selection diversity for dual-polarized antenna systems," *International Journal of Communication Systems*, vol. 33, pp. 1074-5351, Jan. 2020.
[26] L. Xu and Y. J. Zhou, "Low profile high-gain antenna for broadband indoor distributed antenna system," vol. 35, no. 7, pp. 791-796, July 2020.

Hao Xiang Li was born in Xian, Shanxi, China, in 1996. He is currently pursuing the Master's degree of Electronic and Communications Engineering in Shanghai University, Shanghai 200444, China. His research interests include broadband antenna, beaming scanning antenna and metamaterials.

Yong Jin Zhou was born in Shandong, China, in 1982. His current research interests include microwave and millimeter antenna, plasmonic metamaterials and applications, millimeter wave and THz functional devices, wireless energy transmission. He received the B.S. degree in Communication Engineering from Shandong University, Jinan, China, in 2006, and Ph.D. degree in Electromagnetic Field and Microwave Technology from Southeast University, Nanjing, China, in 2011, respectively. From 2009 to 2010, he was a Visiting Scholar of University of Houston. From 2011 to 2012, he was a Software Engineer with EEBU of Marvell Technology (Shanghai) Ltd. From 2012 to 2015, he was an Assistant Professor and from 2015 to 2020, he was an Associate Professor with School of Communication & Information Engineering, Shanghai University, Shanghai, China. Currently, he is a Professor with School of Communication & Information Engineering, Shanghai University, Shanghai, China. He has authored and coauthored over 90 papers in peer-reviewed journals and conference proceedings. He is IEEE Member, OSA Member, and Senior Member of Chinese Institute of Electronics. He is serving as a Reviewer for over 20 peer-reviewed journals, such as Nature electronics, Photonic Research, Optics Letter, Optics Express, Appl. Phys. Express, IEEE Access, IEEE MTT, IEEE MWCL, etc. He was serving as a Session Chair for several International Symposiums.